

High field properties and energy storage in nanocomposite dielectrics of poly(vinylidene fluoride-hexafluoropropylene)

V. Tomer,^{1,3,4,a)} E. Manias,^{2,3,a)} and C. A. Randall^{1,3}

¹Center of Dielectric Studies (CDS), Materials Research Laboratory, The Pennsylvania State University, University Park, Pennsylvania 16802, USA

²Polymer Nanostructures Lab—Center for the Study of Polymeric Systems (CSPS), The Pennsylvania State University, University Park, Pennsylvania 16802, USA

³Department of Materials Science and Engineering, The Pennsylvania State University, University Park, Pennsylvania 16802, USA

⁴The Dow Chemical Co., Corporate Research & Development, Midland, Michigan 48674, USA

(Received 25 May 2011; accepted 10 June 2011; published online 23 August 2011)

Poly(vinylidene fluoride) (PVDF) has generated interest for use in electrical energy storage, mostly due to its high dielectric constant compared to other polymers. There still exist challenges, such as its high energy losses, that have prevented large scale commercialization of PVDF-based capacitors, but progress is continuously being made. In this paper we explore a promising route to improve the energy storage performance of PVDF, through a synergy of HFP comonomers and of kaolinite clay nanofillers. This study shows that the addition of these high aspect ratio fillers to poly(vinylidene fluoride-hexafluoropropylene) [P(VDF-HFP)] copolymers does not increase the polar phase and, consequently, these composites exhibit markedly enhanced dielectric properties at high electric fields. Specifically, strained films of these composites exhibit reduced high field losses, markedly increased breakdown strength and, thus, large recoverable energy density values, in the range of 19 J/cm³. © 2011 American Institute of Physics. [doi:10.1063/1.3609082]

I. INTRODUCTION

Poly(vinylidene fluoride) (PVDF)^{1–3} and, more recently, its copolymers such as those with chlorotrifluoroethylene [P(VDF-CTFE)], hexafluoropropylene [P(VDF-HFP)], and trifluoroethylene [P(VDF-TrFE)], are emerging as potential dielectric materials for advanced applications where high energy density and low loss at high repetition rates are required, such as in grid leveling, rail runs, pulsed lasers, and electric or hybrid vehicles.^{4–6} These ferroelectric polymers exhibit large energy densities, compared to the current state-of-the-art capacitor polymeric films, such as biaxially oriented-polypropylene (BOPP). For instance, copolymer P(VDF-CTFE) possesses a high dielectric permittivity of 13 (1 kHz) and an energy density of ~25 J/cm³ at 620 MV/m, as compared to BOPP that displays an energy density of ~4 J/cm³ at a field of 600 MV/m and a lower permittivity of 2.2 (1 kHz).^{4,7} However, there are still some challenges that need to be addressed before these polymers are commercially utilized. One of the most critical issue is the energy losses due to conduction or hysteresis of ferroelectric switching under high ac fields.

PVDF is a semicrystalline polymer of approximately 50% crystallinity and combines good mechanical properties, chemical resistance, electrical resistance, and processability. PVDF is usually synthesized via free radical polymerization; its backbone (–CH₂–CF₂–) provides for adequate chain flexibility, due to its linear architecture, and additionally promotes specific atomic arrangements, due to the high repulsive forces between the fluorine atoms.^{8–11} This stereochemistry allows for PVDF

to crystallize into at least four phases known as α , β , γ , and δ (or type II, I, III, and VI, respectively),^{2,3,8–12} a crystalline polymorphism which results into versatile dielectric properties for PVDF. The apolar α phase is the dominant phase obtained for PVDF and its co-polymers under usual melt crystallization.¹ However, it is the more polar β -phase that attracts technological interest, since it accounts for the pyroelectric and piezoelectric properties. Accordingly, a lot of research effort has been invested in optimizing PVDF toward yielding materials with high β -phase content. In the simplest approach, the β -phase can be obtained from the non-piezoelectric α -phase by, for example, controlled annealing or mechanical drawing at temperatures ~100 °C. In another approach, it has been shown that crystallization of PVDF from solution, using DMF (dimethylformamide) or DMA (dimethylacetamide), results in a mixture of α and β -phases, and control of the solvent evaporation temperature determines the predominant crystalline phase. More recently, PVDF has been most commonly used in copolymer and terpolymer forms that can be tailored to crystallize in the more polar β -phase for, e.g., poly(vinylidene fluoride-chlorotrifluoroethylene) [P(VDF-CTFE)], poly(vinylidene fluoride-tetrafluoroethylene)[P(VDF-TFE)], poly(vinylidene fluoride-trifluoroethylene) [P(VDF-TrFE)], and poly(vinylidene fluoride-trifluoroethylene chlorotrifluoroethylene) P(VDF-TrFE-CTFE) respectively. In these copolymers, generally, the amount of crystallinity and the desired polar phase can be controlled through the comonomer ratio and processing parameters.^{5,13–15} Not much interest has been devoted to the P(VDF-HFP) copolymers, however, since the presence of HFP does not mediate structural transitions toward ferroelectric PVDF morphologies, as those observed in VDF-TrFE or VDF-TFE copolymers, with the copolymer exhibiting almost

^{a)}Authors to whom correspondence should be addressed. Electronic addresses: vtomer@dow.com and manias@psu.edu.

the same crystal structures as homopolymer PVDF.¹⁶ Recent research has further suggested that the addition of proper nanoparticle fillers, such as organically modified montmorillonite, tends to stabilize the β PVDF phase.¹⁵ This behavior was originally attributed solely to the spatial confinement of the polymer chains, since the macromolecules are sorbed on the flat surfaces of rigid nanofillers, but recent investigations indicate also the possibility of excess β crystal stabilized by charge-dipole interactions.^{17,18} This filler-stabilization of a particular polymer crystal phase in polymer/layered-silicate nanocomposites is not unique to PVDF. In fact, the high performance of the polyamide-6/montmorillonite nanocomposites—which revamped the field of clay-reinforced polymer composites over the past twenty years—has been linked to the clay-stabilized γ crystal phase of polyamide at the silicate surfaces.¹⁹ This behavior necessitates strong interactions between the polymer and the SiO_x cleavage plane of the silicate, for example, through hydrogen bonds—as is the case with polyamide¹⁹ and polyvinyl alcohol²⁰—or through electrostatic interactions between a polar polymer and the dipoles in the silicate—as is the case with PVDF and montmorillonite.^{17,18} Therefore, in order to design clay-reinforced PVDF composites with reduced β phase, and/or with a preferential stabilization of the non-polar α phase, it is obvious that a layered silicate with smaller dipole/charge density than montmorillonite should be employed, as, for example, kaolinite or talc. This approach would capitalize on the thermomechanical reinforcement of PVDF by the nanofiller,²¹ without sacrificing the dielectric performance in the final composite; actually, in this case, complete filler dispersion (exfoliation) is probably not required, and high performance would be expected by PVDF in both “genuine nanocomposite”, as well as in “nanofilled” polymer structures.²² Irrespectively of the mechanism in effect, almost any inorganic nanofiller particle will act as a heterogeneous nucleating-agent for the PVDF crystallization; thus, the performance optimization for such composites would necessitate controlling the filler-induced crystal phase.²³

This work aims in capitalizing on the synergy of hexafluoropropylene (HFP) comonomer and kaolinite clay nanofillers in PVDF, toward improving the high-field dielectric response of these composites’ strained films. In contrast to other layered-silicates, such as organo-montmorillonite, it is seen here that kaolinite fillers do not promote the polar β phase in these PVDF-copolymers. Our results further indicate that this comonomer/filler combination results in a conduction barrier and, hence, in improved high-field losses and a strongly increased breakdown strength, far beyond what can be achieved by the unfilled copolymer films, even under optimized annealing and mechanical straining. Finally, this work also explores the capacitive energy storage performance of these composites, reporting one of the highest recoverable energy densities recorded for solution-cast PVDF-based films.

II. EXPERIMENTAL

A. Materials and sample preparation

Poly(vinylidene fluoride-co-hexafluoropropylene), referred hereafter as P(VDF-HFP), is a random copolymer with

10% HFP co-monomer, supplied by Solvay-Solexis (Solef 11010/1001, 61 wt. % fluorine content). The inorganic kaolinite fillers (Burgess KE[®], nominal particle size 1.5 μm , CAS 92704-41-1) used in this study were obtained from Burgess Pigment USA, and they are fully calcined clays with an x-ray-amorphous structure containing defect spinel inclusions. The Burgess KE filler was surface treated, so as to improve its interfacial properties, with (3-mercaptopropyl)trimethoxysilane (Gelest) as follows: 10 g of Burgess KE powder were suspended in a solution of 90 ml ethanol, 10 ml distilled water and 0.6 g of (3-glycidoxypropyl)trimethoxysilane. The obtained mixture was vigorously stirred for 24 h, subsequently centrifuged for 10 min and finally the precipitated modified powder was dried at 120 °C overnight.

PVDF-HFP/kaolinite nanocomposites were made by the co-precipitation method. For the co-precipitation method, 5 wt. % PVDF-HFP solution in N, N-dimethyl formamide (DMF, Sigma Aldrich) was mixed with the appropriate amount of DMF suspension of Burgess KE (the suspension had been subjected to vigorous stirring overnight, followed by ultrasonication for 30 min). The mixture was vigorously stirred for 24 h, and subsequently used to cast films (50–60 μm) on glass plates (5 × 3 type). The glass plates were dried at 70 °C for 6 h. The films were then peeled off the glass substrate and further dried (to ensure the complete removal of the solvent) in vacuum oven at 80 °C over a period of 10 h followed by a 5 h oven-drying at 115 °C.

Finally, the films were hot-pressed at 200 °C and 55 MPa (8000 psi) pressure for 10 min and then were left to crystallize at room temperature. The resultant films were then uniaxially stretched mechanically by means of a zone drawing process to five times their original length (draw ratio: 5 ×; strain: $\epsilon_x = 400\%$; stretch ratios: $\lambda_x = 5$, $\lambda_y = 1$, $\lambda_z = 0.2$). The equipment used for stretching utilized a very narrow heating-zone (set at 100 °C) and the drawing ratio was precisely controlled by the differential speed of the two motors attached to either end of the stretching stage.²⁴ Lastly, the stretched films were annealed at 120 °C for 6 h before electrical measurements.

B. Instrumentation

1. X-ray diffraction

Wide angle x-ray diffraction (XRD) measurements were carried out by using a PANalytical/X’Pert Pro MPD X-ray diffractometer (45 kV, 40 mA) using Cu K_α radiation ($\lambda = 1.5418 \text{ \AA}$) in the 2θ range 0°–30°. All XRD data were imported to “PEAKFIT” software and a deconvolution of the peaks was performed by fitting to a superposition of Gaussian functions, allowing for determination of the integrated peak areas and refinement of the peak positions.

2. Transmission electron microscopy

A Leica Ultracut UCT Microtome with cryo-attachment was used for sectioning the specimens. The microtomed samples were mounted on copper grids and observations of microstructure were made using a Jeol JEM-2010 Transmission

Electron Microscope, with LaB6 emitter, operated at 200 KV accelerating voltage.

3. Infrared spectroscopy

Fourier transform infrared spectroscopy (FT-IR) was carried out on a Bruker IFS 66/S FT-IR spectrometer. Spectrums were obtained in the attenuated total reflectance mode by using a ZnSe crystal in contact with the sample surface. The angle of the incidence infrared beam was 45 degrees and data were collected by sampling over four different spots on both sides of the specimen.

4. Differential scanning calorimetry

DSC data were collected on a TA Q200 calorimeter in a gas mixture of nitrogen and helium. The measured heat flow was obtained in the conventional mode at heating and cooling temperature ramps of 10 °C/min. The temperature accuracy was 0.1 °C. For the data analysis, the TA universal analysis software was used.

5. Dielectric characterization

The dielectric properties were measured at 1 kHz from –50 to 110 °C using a HP4284 LCR meter (Palo Alto, CA) while samples were heated at 4 °C/min in a computer-controlled oven. Gold electrodes of 3.3 mm diameter and a typical thickness of 60 nm were sputtered on both sides of the stretched films (~10–12 μm thick) for the electrical measurements.

6. Displacement-electric field loops

High-field polarization-electric field loops were recorded with a modified Sawyer–Tower circuit. The samples were subjected to a unipolar wave, with frequency of 10 Hz. The polarization-electric field loops are presented according to the data from the first cycle.

7. Dielectric breakdown strength

Dielectric breakdown measurements were performed on a TREK P0621P instrument. An electrostatic pull-down method was used to measure the breakdown field, where a voltage ramp rate of 500 V/s was applied between a rounded electrode and the gold-coated polymer film.²⁵ HALT (Highly Accelerated Lifetime Testing) data was obtained at 500 V at 50 °C and comparisons were made to a commercially obtained BOPP polypropylene film; the HALT test was stopped after 180 h (648 × 10³ s) if no failure of the film specimen occurred.

III. RESULTS AND DISCUSSION

A. Structural analysis

The XRD patterns of at least four PVDF crystal phases (α , β , γ , and δ) have been widely reported in the literature.^{2,3,8–12} PVDF's chain architecture allows for a crystalline orthorhombic unit cell (β -phase) with two planar zigzag chains passing through it and a space group of Cm2m(C_{2v}^{14}),

which upon relaxation of the intrachain steric hindrances can lead to a less dense P2₁/c(C_{2h}^5) monoclinic crystal (α -phase), both these were investigated by several groups in the 1960s and 1970s.^{8–11} The relevant Bragg diffractions detected here for P(VDF-HFP) and its 5 wt. % kaolinite nanocomposite are shown in Fig. 1. At the outset, it is seen that the 10 mol % of HFP comonomer does not significantly change the lattice symmetry compared to PVDF homopolymer;^{11,16} hence, the XRD patterns of PVDF/HFP copolymer can be analyzed^{16,26} in reference to the standard XRD patterns for PVDF.^{2,3,8–12} FT-IR analysis excludes the presence of a marked γ -phase in our systems (see next), thus the various diffractions seen in Fig. 1 can be indexed according to the α and β PVDF crystal phases. Of interest here are the peaks at $2\theta = 17.7^\circ$, 18.4° , 19.9° , and 26.5° corresponding to the 100, 020, 110, and 021 diffractions, respectively, all from the PVDF α -phase, as well as the $2\theta = 20.8^\circ$ peak that corresponds to the superposition of the 110 and 200 β -phase diffractions.

The XRD patterns for as-cast/unstretched P(VDF-HFP) films and its nanocomposites show qualitatively similar behavior with that of PVDF, signifying the presence of primarily nonpolar α -phase. Quantitatively, however, it is obvious that the peak intensity ratios of the copolymer differ from that of the PVDF homopolymer's α -phase, indicating a different crystalline structure: For example, the XRD patterns of P(VDF-HFP) show greater intensity at the 020 peak than the 110 peak, while the reverse is true for PVDF homopolymer. As the films are subjected to uniaxial straining, to five-times their original length, the diffraction patterns indicate a conversion of the crystalline structure to more polar β , at the expense of the nonpolar α -phase. This is reflected by the disappearance of the 021 α -phase peak, together with a depression and broadening of the (020) α and (110) α in the unstretched sample, and the evolution of the (110,200) β peak at 20.8° . This XRD signature is characteristic of α to β transformation for PVDF homopolymer.^{3,12,27}

Regarding the influence of the kaolinite filler on the polymer crystallinity, it has been widely suggested that layered silicate nanoparticles (e.g. clays) tend to favor the evolution of and stabilize the β phase in PVDF and its copolymers. This has been originally related to the spatial confinement of the polymer chains imposed by the rigid nanofillers,¹⁵ a tendency that can be amplified by charge-dipole interfacial interactions.¹⁷ The influence of the silane-modified kaolinite filler used here does not seem to markedly promote the evolution of additional β phase, neither in the unstretched, nor in the stretched films, as is obvious by comparing the XRD traces of unfilled versus 5 wt. % composite films (Fig. 1); if anything, in both cases the kaolinite seems to strengthen the diffractions that correspond to the α -phase, i.e., the 110 α for the unstretched films and the 021 α for the strained films. More quantitatively, this effect of the kaolinite on the PVDF crystallinity can be quantified through the composition of the crystalline phase, e.g., through the fraction of β -phase F_{β}^{XRD} , which, in a first approach, is $F_{\beta}^{XRD} = A_{\beta}/A_C$ (where A_{β} is the total area of peaks assigned to the β -phase and A_C is the total area of all crystalline peaks). The stretched nanocomposite films showed very similar β -phase crystallinity values to the unfilled P(VDF-HFP)

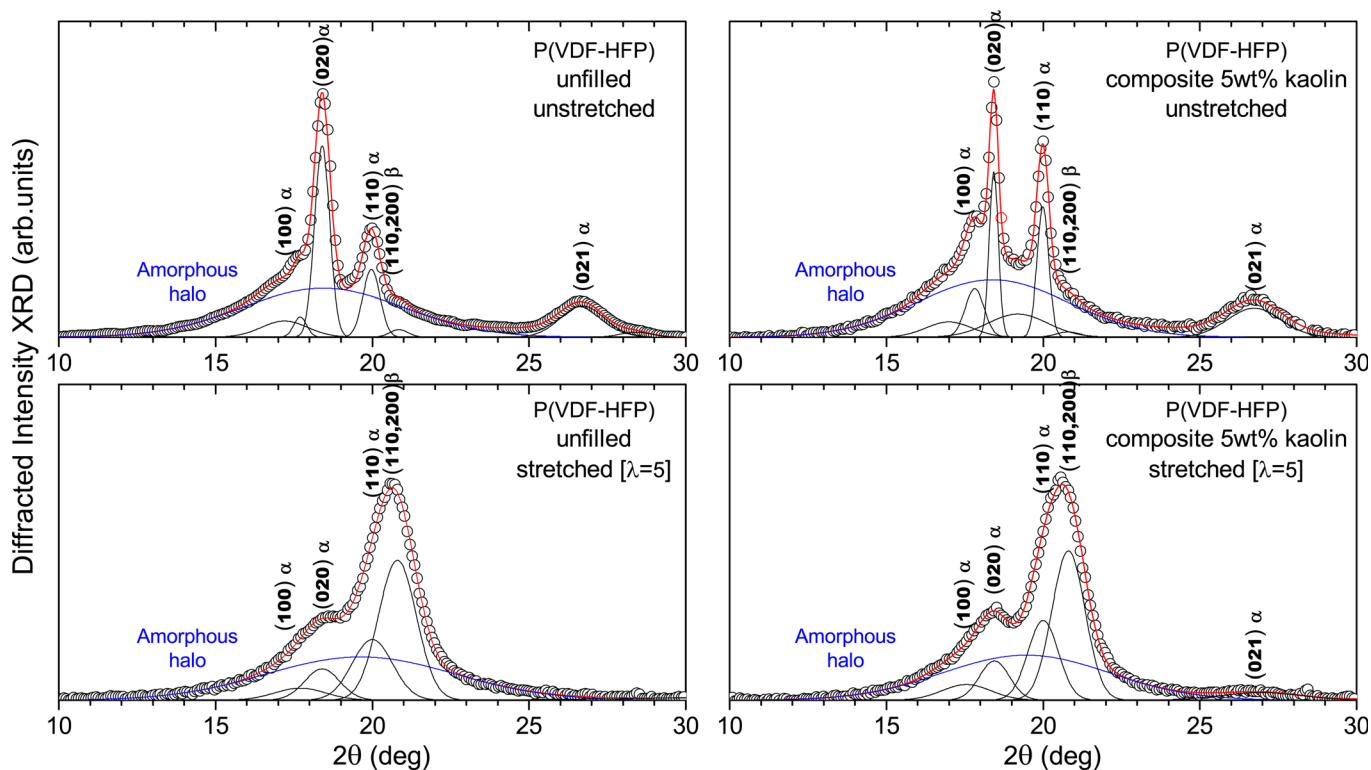


FIG. 1. (Color online) Comparison of wide-angle x-ray diffraction patterns for the P(VDF-HFP) copolymer films: as cast (top, unstrained) vs strained (bottom, stretched, $\lambda_x = 5$), as well as unfilled (left) vs composites (right, 5 wt. % kaolinite). XRD signatures of α and β crystalline phases of PVDF are identified; mechanical strain results in a high-degree of α to β conversion for both unfilled and composite films, whereas the addition of kaolinite does not have a marked effect (in either stretched or unstrained films).

of about 29%, which again suggests that the introduction of the inorganic filler does not introduce marked changes in the P(VDF-HFP) crystal structure. These results are quite promising since β -phase in excess 30% result in high ferroelectric losses that can overshadow any other advantages gained by mechanical straining or annealing of these films.

Given the overlapping XRD peaks of the α and β phases, as well as the possibility of the γ phase manifesting upon stretching,¹² the above XRD analysis is inherently rather approximate. Therefore, the XRD structural analysis for unstrained and stretched samples of P(VDF-HFP) and its nanocomposites was complemented by infrared spectroscopy. Figure 2 demonstrates the differences in absorption peaks of the stretched and unstrained copolymer, along with their respective nanocomposites. The results here are consistent with the XRD results in that: (i) the introduction of kaolinite nanofiller does not qualitatively alter the FT-IR spectra of P(VDF-HFP) and (ii) the application of stretching results in an increase in β -phase and an associated decrease in α -phase, for both the unfilled P(VDF-HFP) and the nanocomposites. Specifically, focusing on the 700–900 cm^{-1} region, the absorption peaks at 764 and 796 cm^{-1} are exclusively present in the α PVDF phase, the γ band would have had absorption peaks at 776 and 812 cm^{-1} (both of which are completely absent), and, in absence of γ , the 840 cm^{-1} band is exclusively due to the β phase. Thus, the spectra clearly indicate that there are only α and β phases coexisting in our films, with no measurable γ phase. Further, using the absorptions at 764 and 840 cm^{-1} as the characteristic peaks for the α and β -phase, cf. associated with the TGTG and TTTT conformations, respec-

tively,^{12,28} we can quantify the relative fraction of the two crystalline phases: Across all unstrained samples, a large excess of α is clearly evident, and there is no measurable conversion of the α phase upon addition of the nanofiller (in any of the three filler concentrations studied, 1–5 wt. %). Upon stretching, all α -phase absorption peaks decrease across all systems—although α still remains the predominant

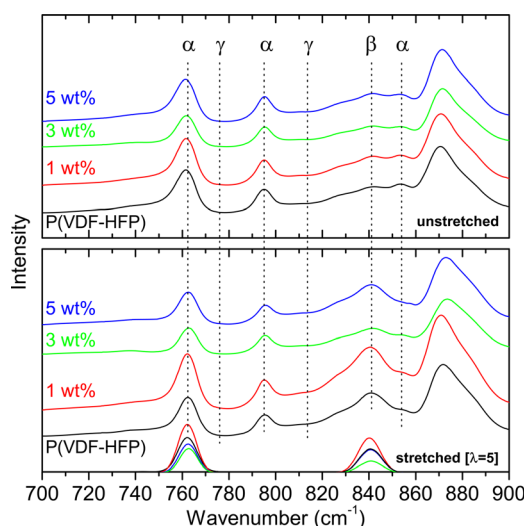


FIG. 2. (Color online) FT-IR spectra of P(VDF-HFP) copolymer and its 1, 3, and 5 wt. % nanocomposites: Attenuated total reflection intensities from stretched (bottom) and as-cast (top, unstrained) films. The γ -exclusive absorptions at 776 and 812 cm^{-1} are absent in all systems. For the stretched films, the background-corrected fits for the α -764 cm^{-1} and β -840 cm^{-1} absorption peaks are also shown.

phase—with a simultaneous increase in the β -phase band at 840 cm^{-1} . Finally, comparing between the stretched films, there is no systematic dependence of the β absorption intensity on the filler concentration, with the 1 wt. % composite showing the highest β absorption, the 3 wt. % showing the lowest, and the 0 and 5 wt. % being intermediate. To quantify the relative content in β -phase, a series of peak heights were determined by simulating the observed spectrum using the OPUS data analysis software, which automatically corrects for the baseline (the 764 and 840 cm^{-1} fitted-peaks are also shown in the inset of Fig. 2). In each sample, the fraction of the β crystalline phase (F_{β}^{IR}) was calculated^{29,30} by $F_{\beta}^{IR} = A_{\beta} / (1.26A_{\alpha} + A_{\beta})$,³¹ where A_{α} and A_{β} are the corresponding absorption bands (peak heights at 764 and 840 cm^{-1}) and the 1.26 factor accounts for the ratio in absorption coefficients at 764 and 840 cm^{-1} . The calculated values of F_{β}^{IR} for the unfilled stretched copolymer and its nanocomposites were all found to be in the range of 28–38% for the composites compared to 33% for the unfilled matrix, in good agreement with the x-ray diffraction results.

DSC thermographs (first heating and cooling cycles, unstretched samples) of the three nanocomposites are compared with the unfilled polymer in Fig. 3. The DSC endotherms of the P(VDF-HFP) display an asymmetrical melting peak at $T_m = 158\text{ }^{\circ}\text{C}$, about $10\text{ }^{\circ}\text{C}$ lower and slightly broader than the melting peak of an $\alpha + \beta$ PVDF homopolymer;¹² the T_m depression is probably due to the HFP comonomer and the broadening due to compositional drifts in the copolymer.¹⁶ Namely, although the copolymer has on average a 10% HFP comonomer, which is sufficient to reduce the T_m , at the same time, there is a quite broad distribution of copolymer compositions, i.e., of the HFP content across the system polymers, as is typical with free radical copolymers; this distribution of compositions evidently results in varied crystalline structures and morphologies (viz. the deviations reported above in the XRD 020 and 110 α diffraction peaks) and an associated distribution of melting points (viz. an asymmetrical broad peak in the DSC melting endotherms). The addition of kaolinite did not affect the melting behavior of the copolymer, and the melting peaks retain the same shape and peak temperature for 1–5 wt. % added filler. This is consistent with the XRD and FT-IR results above, where no marked changes in the crystal structure were observed upon addition of the kaolinite. However, the nanocomposites exhibited a slightly larger enthalpy of melting (about 28 J/g) as compared to the unfilled P(VDF-HFP) matrix (about 23 J/g), denoting a slightly higher polymer crystal fraction for the nanocomposites. Where there do exist marked changes upon composite formation are the DSC cooling traces: Namely, all DSC cooling-cycle traces show a higher crystallization temperatures for the nanocomposites ($T_c = 131.8\text{--}132.5\text{ }^{\circ}\text{C}$, increasing with kaolinite loading) compared to the unfilled polymer ($T_c = 127\text{ }^{\circ}\text{C}$). This $5\text{ }^{\circ}\text{C}$ increase in T_c is a clear manifestation of the kaolinite acting as a heterogeneous nucleating agent for P(VDF-HFP); the very slight increase observed across composites ($\Delta T_c \sim 0.5\text{ }^{\circ}\text{C}$ for 1 to 5 wt. % filler) maybe due to changes in thermal conductivity upon addition of the filler, similarly to other polymer/clay nanocomposites. Accordingly, given the common thermal history used for all sample/film preparations, this higher T_c

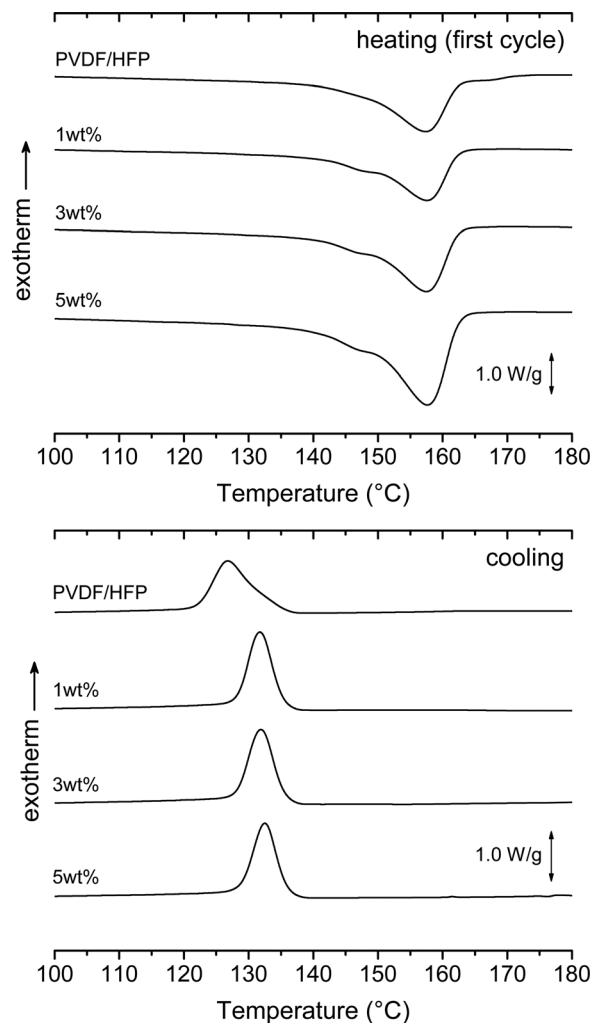


FIG. 3. (Top) DSC data from first heating at $10\text{ }^{\circ}\text{C}$ per minute for unstretched P(VDF-HFP) and various composites; there is no marked change in the melting peak region signifying a common crystalline structure. These DSC traces correspond to the films as tested for dielectric properties. (Bottom) DSC traces of the subsequent cooling cycle of the same systems; the shift of the crystallization peak at higher temperatures suggests a heterogeneous nucleation effect by the kaolinite fillers.

for the nanocomposites also naturally accounts for the higher enthalpy of melting observed in the first heating-cycle of the DSC.

A direct observation of the fillers' position with respect to the P(VDF-HFP) crystals can be obtained by TEM (Fig. 4). Comparison of bright and dark field TEM imaging shows a clear tendency of lamellae type of growth close to, and probably initiated by, the kaolinite fillers, consistent with the higher T_c observed in DSC. Thus, consideration of all information above shows that the kaolinite nanofillers do not alter the crystal structure of the polymer and do not markedly promote excess formation of the β phase (in either the as-cast or the stretched films, cf. XRD, FT-IR, and DSC heating), despite their action as heterogeneous nucleating agents for this copolymer (cf. DSC cooling and TEM). Thus, if anything, for the composites studied here the selected silane-treated kaolinite is expected to stabilize the α phase of PVDF in the vicinity of the fillers. This effect of the nanofillers on the polymer's crystal nature, coupled with the expected mechanical

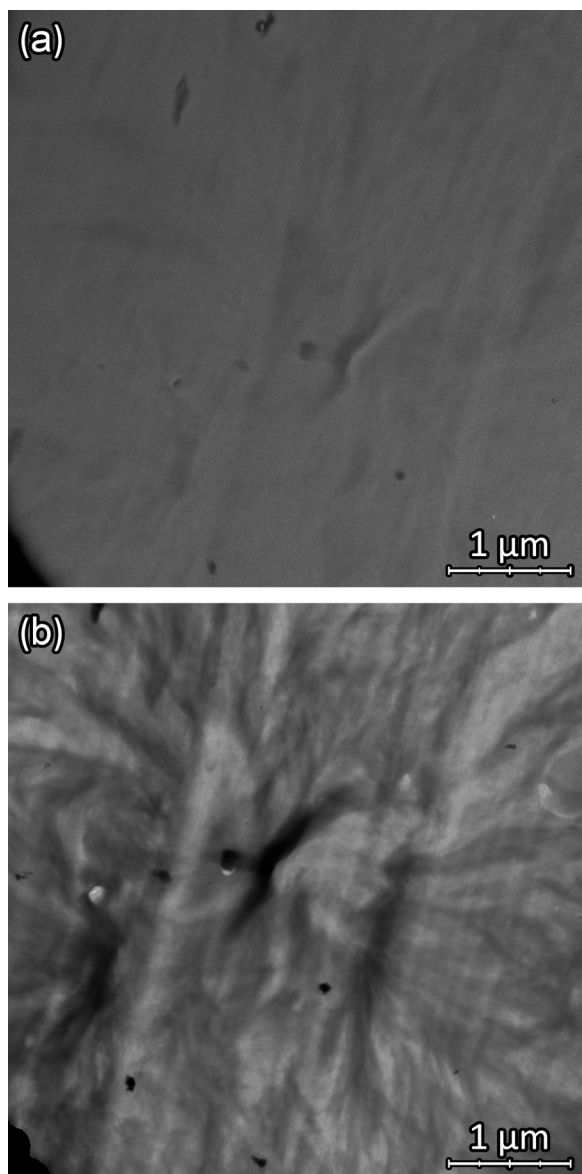


FIG. 4. (a) Bright field and (b) dark field TEM images from the same region of a PVDF-HFP nanocomposite containing 5 wt. % kaolinite. Polymer crystal lamellae are observed close to, and radiating away from, the fillers (dark elongated features in the bright field); this behavior is seen throughout the TEM observed specimens, and is consistent with a heterogeneous nucleation of polymer crystals from the inorganic nanofillers.

reinforcement, is expected to play an important role in determining the dielectric properties of the nanocomposites, as discussed in later sections.

B. Dielectric characterization

1. Low-field measurements

The temperature dependence of the dielectric permittivity (ϵ') and of the dielectric loss tangent ($\tan \delta = \epsilon''/\epsilon'$), at 1 kHz, is shown in Fig. 5 for strained films of unfilled P(VDF-HFP) and 1 and 5 wt. % kaolinite-reinforced nanocomposites. Qualitatively, the low-field response of the copolymer and its composites resemble closely the response of PVDF: The dielectric loss shows a major peak at about -25°C that corresponds to the glass transition. There is also a much smaller

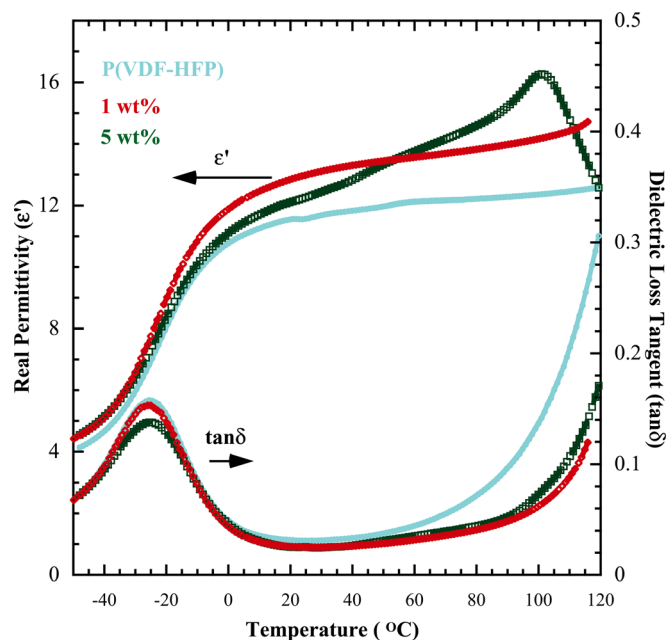


FIG. 5. (Color online) Dielectric permittivity (ϵ') and dielectric loss tangent (ϵ''/ϵ') vs temperature, at low electric field and 1 kHz, for the stretched films ($\lambda_x=5$) of unfilled P(VDF-HFP) and two nanocomposites with 1 and 5 wt. % kaolinite.

peak at approximately 60°C and an associated step in ϵ' for all stretched samples, which is not reversible upon cooling. This is a known PVDF relaxation, whose origin has been related to an interfacial polarization of the amorphous-crystalline boundaries, and to relaxations of the rubbery (amorphous) domains of the polymer.^{32–34} A third peak, detected at a temperature of about 110°C , and predominately featured for the higher filler loading composite, is believed to be linked to movements within the crystalline regions coupled with motions of the folds.³⁴ Given the prior published works, and since this work is mostly focused on understanding the high field dielectric behavior and energy storage, the mechanisms behind the low-field relaxations will not be discussed in more detail here. However, it is important to note that upon nanocomposite formation there is a marked improvement in the high temperature dielectric loss, compared to the unfilled stretched P(VDF-HFP) films. This behavior signifies a substantially decreased space charge conduction at high temperatures in the composites. At first sight, this is in concert with the expected composite's barrier to conduction (i.e., barriers due to high aspect ratio fillers arranged perpendicular to the direction of the applied field), in addition to any polymer crystallization effects, such as a higher crystallinity and an enhanced ordering of the crystallites in the composites. Both these effects can play a major role in improving the high field performance of the polymer.^{35,36}

2. Displacement-electric field loops

High field performances of these nanocomposite materials were evaluated by obtaining a series of displacement-field loops (D-E loops), that is, by measuring the electric displacement field ($\vec{D} \equiv \epsilon \vec{E} + \vec{P}$; where D is the electric displacement; E is the applied electric field; and P is the polarization) versus

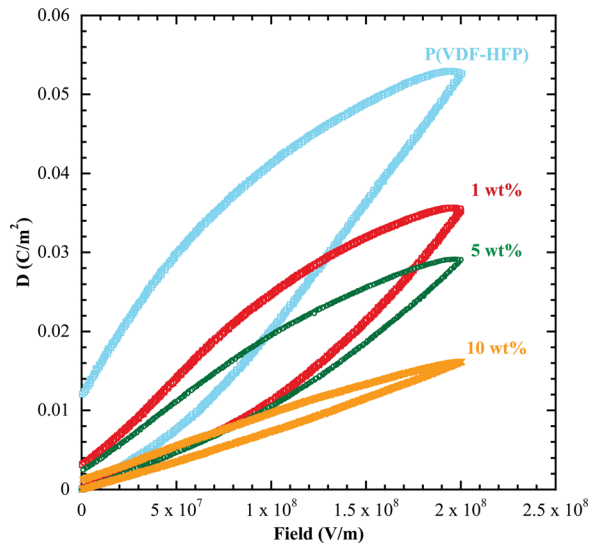


FIG. 6. (Color online) Displacement vs electric field loops of P(VDF-HFP) and of its nanocomposites; all films were uniaxially stretched ($\lambda_x = 5$). Upon kaolinite filler addition there is a systematic reduction in remnant polarization and an associated improvement in losses.

the applied electric field. The electric displacement hysteresis loops, measured for stretched films of P(VDF-HFP) copolymer and its nanocomposite with 1, 5, and 10 wt. % kaolinite, are shown in Fig. 6. The unfilled P(VDF-HFP) films showed the highest polarization at any field compared to the nanocomposites. In addition, the observed remnant electric displacement in stretched P(VDF-HFP) is found to be much smaller than the value of pure β -phase PVDF. This could be due to the HFP comonomers along the PVDF chains that can act as effective defects to destabilize the ferroelectric β -phase. The polarization values in the unfilled P(VDF-HFP) samples were also accompanied by large high-field losses. The origins of such losses, in PVDF, have previously been related to ferroelectric switching and space charge conduction present at high fields.^{37,38}

Upon addition of kaolinite nanofillers, a systematic reduction in remnant polarization—accompanied by an associated improvement in losses—was observed for the composites (Fig. 6), with the lowest values for dielectric

displacement and for losses recorded for the 10 wt. % composite across all fields.³⁹ The origin of these low displacement (D) values for the nanocomposites can be rationalized by the simultaneous presence of two mechanisms: First, the surface treated high surface ratio fillers act as nucleating centers, as suggested above, promoting growth of non-polar crystals in their vicinity, which now require higher fields for dipole reorientation due to their more restricted mobility. Second, the filler-induced reduction in oriented dipole density will dictate a lower amount of space charge required for polarization stabilization, as suggested by the charge trapping model in P(VDF-HFP) copolymer nanocomposites.⁴⁰ These two mechanisms, acting simultaneously, can account for both the reduction in observed displacement values and the reduced losses present in the D - E loops (opening of loops in Fig. 6); this combination of low displacement and losses is generally related to an improved dielectric breakdown behavior. Furthermore, the high aspect ratio kaolinite can provide for efficient conduction barrier in these textured nanocomposites; namely, both fillers and interfaces within the composite can limit the charge migration toward the electrodes and, thereby, substantially reduce the high space charge losses observed in the respective unfilled copolymer.

3. Dielectric breakdown

The electrical breakdown results, Fig. 7, were analyzed by a two-parameter Weibull distribution function: $P(E) = 1 - \exp[-(E/\alpha_w)^{\beta_w}]$, where $P(E)$ is the cumulative probability of failure occurring at the electric field lower or equal to E . The α_w scale parameter is the field strength for which there is a 63% probability for the sample to break down, while the shape parameter β_w evaluates the scatter of data.³⁶ Figure 7 clearly demonstrates the increased breakdown strength exhibited by the 5 wt. % nanocomposite compared to the respective unfilled polymer. This nanocomposites shows a marked 50% improvement in breakdown strength compared to the respective unfilled PVDF copolymer (α_w increases from 530 MV/m for the unfilled copolymer film to 780 MV/m for the composite films, with similar shape parameters). In addition, these nanocomposites showed an improved “graceful

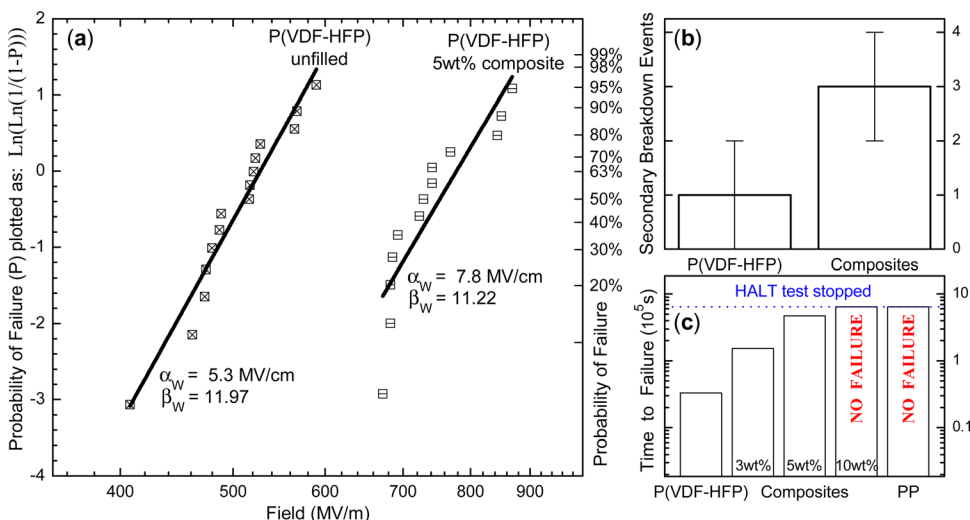


FIG. 7. (Color online) (a) Weibull distribution and observed dielectric breakdown strength of stretched P(VDF-HFP) and 5 wt. % nanocomposite sample. Also, shown is the (b) typical number of allowed voltage cycles (graceful failure type behavior) and (c) HALT data (500 V at 50°C, stopped after 180 h) benchmarking the performance of P(VDF-HFP) and its nanocomposites against high-performance BOPP polypropylene films.

failure” mechanism showing a larger number of secondary breakdown events compared to the matrix polymer (Fig. 7(b)). Despite the small electrode size, the same composite film specimen could be cycled through the breakdown voltage level, at least twice or more, indicating a more localized failure for the unfilled P(VDF-HFP) films, compared to a more tortuous and more branched electron tree formation in the composite. We expect that the observed graceful failure can be further optimized with proper choice of electrode chemistry and thicknesses profiles. In concert with this graceful failure behavior, this improved reliability of the nanocomposites compared to the unfilled PVDF copolymer is also reflected in the Weibull distribution of failure (Fig. 7). Namely, the complete failure distribution curve of the nanocomposite lies at higher applied field values, well-above the 99% probability of failure, corresponding to the unfilled PVDF-HFP, while it retains the same value of the shape parameter β_w . That is, the 5 wt. % nanocomposite films do not exhibit any dielectric breakdown failure even for field-strengths well-above the 600 MV/m, where all the respective PVDF copolymer films have definitively failed ($P > 99\%$).

The above breakdown strength results were further validated by HALT data (highly accelerated lifetime testing), illustrated in Fig. 7(c), that shows a systematic improvement in time to failure for the nanocomposites compared to the unfilled P(VDF-HFP) films. Nanocomposites with 5 and 10 wt. % filler loading actually showed comparable time to failure as a commercial high-performance linear dielectric film (bi-oriented polypropylene, PP). On this last point, the onset of electromechanical failure (stresses induced by the applied field exceed the yield stress of the polymers, causing a rapid inward collapse of the electrodes and electrical discharge) has been reported as a trigger mechanism for the failure in PVDF and its copolymers.⁴¹ Along these lines, and in concert with earlier work in PVDF/clay nanocomposites,²¹ the presence of aligned surface-modified kaolinite fillers is expected to improve the mechanical properties, compared to the unfilled polymer, and to give rise to a filler network that has a protective role against the onset of catastrophic failure, even in absence of high nanometer-scale dispersion.^{23,35} In fact, absence of kaolinite exfoliation accounts very naturally for the systematic increase in time to failure with filler loading (Fig. 7(c)), since the filler percolation threshold is expected to move above 10 wt. % filler. This supposition—albeit extrapolating from a different layered-silicate nanofiller—does support our measured breakdown performances, and is herewith offered as an explanation for the observed behavior.

4. Recoverable energy density and efficiency

The recoverable energy density at any field can be obtained by integration of the area between the D-E loop curve and the corresponding field strength ordinate.^{36,42} This recoverable energy density is presented as a function of applied field in Fig. 8. The 5 wt. % nanocomposite shows a significant increase in the maximum recoverable energy density, more than double that of the unfilled polymer matrix (19 J/cm^3 compared to 9.8 J/cm^3). This marked improvement is due to the composite’s low high-field losses and, primarily,

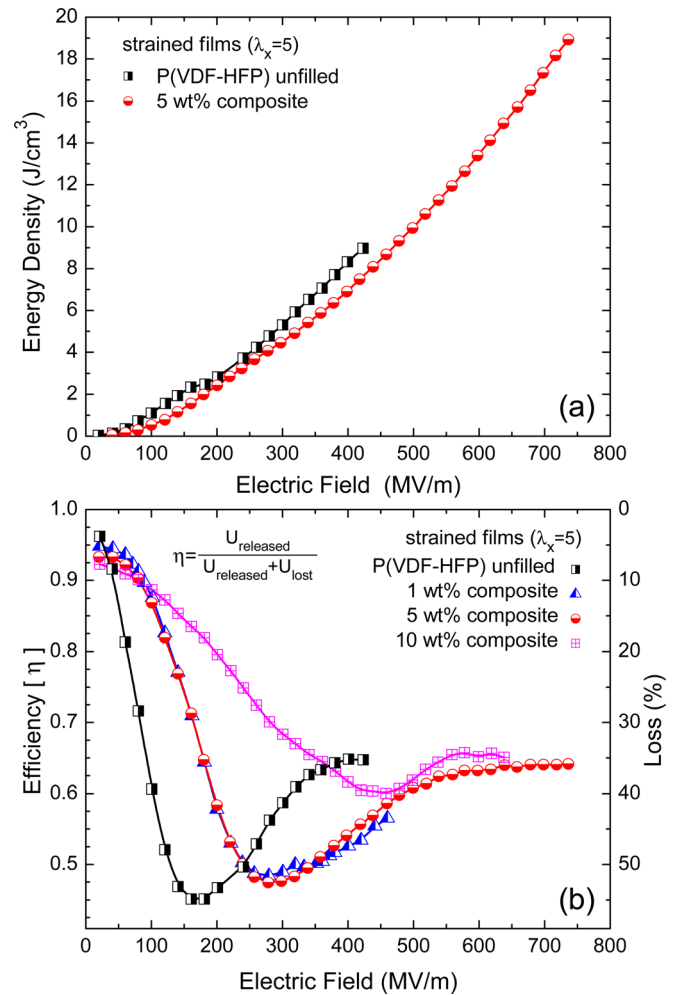


FIG. 8. (Color online) (a) Calculated recoverable energy density from the D-E loops of Fig. 6, comparing the unfilled stretched P(VDF-HFP) films against its 5 wt. % kaolinite composite; there is a marked increase in the max recoverable energy density primarily due to an increase in the breakdown strength. (b) The corresponding system efficiencies for stretched films, of unfilled P(VDF-HFP) and its 1, 5, and 10 wt. % nanocomposites.

due to its higher breakdown strength, and clearly reflects a synergy between the kaolinite fillers and the HFP comonomer, outperforming the relative improvements that can be achieved by electrical or mechanical manipulation of cast P(VDF-HFP) films.¹⁶ For practical applications, beyond a high energy density, it is highly desirable to maintain also a high efficiency (η), or equivalently low loss, since losses lead to heating and, consequently, to detrimental effects on the performance and reliability of the capacitors. In general, for a typical polarization-field response, as illustrated in Fig. 6, the various system energies correspond to the corresponding D-E areas: the released energy U_R is the area between the loop and the corresponding ordinate, the energy loss U_L is the area inside the loop, and the sum of U_R and U_L denotes the total stored energy ($U_S = U_L + U_R$). The efficiency of the system can be defined as ($\eta = 1 - U_L/U_S = U_R/U_S$). Since ferroelectric materials are non-linear materials, their losses change with the applied field, because of field-dependent loss mechanisms.⁴³ This results in the considerable difference between the weak field and high field losses and, thus, efficiencies. As the field increases further—particularly above 100 MV/m—a

significant increase in loss was observed across all systems, unfilled P(VDF-HFP) and its kaolinite nanocomposites, with a definitive loss peak at 200 to 400 MV/m field, depending on system (Fig. 8). Such a non-linear effect in ferroelectric materials is often associated with the ferroelectric switching by applied fields.⁴⁴ Evidently in P(VDF-HFP)—despite the stabilization of the non-polar phase by the addition of HFP comonomer—there still remains some degree of local field induced polarization switching from non-polar to polar conformations, which leads to the ferroelectric switching loss. However, the non-polar to polar change is only partially reversible after the mechanical stretching of the films, and the presence of residual polar conformations leads to significant ferroelectric switching loss.¹⁶ This behavior is reduced by the nanocomposite formation, due to further stabilization of the non-polar α -phase as stated earlier, a trend which is clearly evident in a shift of the loss peak to higher fields with increasing filler loading (Fig. 8(b)).

Along these lines—and considering the combined picture of energy storage, high field losses, and breakdown strength—the synergy of kaolinite nanofillers and HFP comonomers is having an effect on the dielectric properties of PVDF, which is reminiscent of that of cross-links: Specifically, both the trends and the magnitude of improvement across these dielectric properties are consistent with what can be achieved by optimized cross-linking of P(VDF-CTFE), one of the highest performance cross-linked PVDF copolymer systems.⁴⁵ In this sense, the kaolinite nanofillers, by virtue of the copolymer physisorption on their surfaces, can be considered as homologous to “physical crosslinks” in PVDF, increasing the breakdown strength and remnant polarization—and thus also increasing the max recoverable energy density; in addition, the presence of the HFP comonomer evidently stabilizes the α -phase and leads to a reduction of high-field losses, further improving the high field performance. Assuming that this physical explanation is valid, one can naturally justify why the present P(VDF-HFP)/kaolinite composite films outperform what can be achieved by unfilled P(VDF-HFP) films, even when the latter are optimally treated (annealing and straining are optimized¹⁶).

IV. CONCLUSIONS

The effects of uniaxial stretching and addition of a high aspect ratio nanofiller on the energy storage capabilities of P(VDF-HFP) copolymer have been investigated. Similar to what is observed in PVDF, mechanical strain promotes a partial conversion of the primarily non-polar α crystalline structure of the cast copolymer films to the more polar β phase, generally associated with high field ferroelectric losses. However, in contrast to other homologous layered-silicates, such as montmorillonite, the addition of kaolinite fillers does not further promote the formation of the polar β -phase. If anything, XRD, FT-IR and DSC studies indicate that these fillers stabilize the non-polar α phase in the strained films. The synergy of this filler effect and of the HFP comonomer gives rise to a very attractive dielectric property set: At low electric fields the permittivities of the nanocomposites were found to be comparable to that of the unfilled copolymer

films. At high electric fields the same nanocomposites showed enhanced high field losses, and, in particular, a marked increase in dielectric breakdown strength, also exhibiting more graceful failure and substantially longer times to breakdown. In addition, due to their enhanced breakdown strength, the kaolinite-filled composites showed concomitantly higher maximum recoverable energy densities—more than twice the value of the respective unfilled copolymer films—while maintaining a high energy storage efficiency. The improved high-field dielectric performance of these composites was tentatively attributed to kaolinite fillers' ability to impede the copolymer's reorientation under electric field. Irrespective of the physical origin responsible, the recorded concurrent improvements in the composites' dielectric characteristics, if further optimized, could have a profound impact on the development of future high-energy storage polymer capacitors.

ACKNOWLEDGMENTS

This work was supported by the Office of Naval Research (Grant No. MURI-00014-05-1-0541); E.M. acknowledges additional financial support by the National Science Foundation (Grant No. DMR-0602877).

¹The Applications of Ferroelectric Polymers, edited by T. T. Wang, J. M. Herbert, A. M. Glass (Chapman and Hall, New York, 1988).

²Ferroelectric Polymers: Chemistry, Physics, and Applications, edited by H. S. Nalwa (Marcel Dekker, New York, 1995).

³A. J. Lovinger, *Macromolecules* **14**, 322–325 (1981).

⁴X. Zhou, B. Chu, B. Neese, M. Lin, and Q. M. Zhang, *IEEE Trans. Dielectr. Electr. Insul.* **14**, 1133–1138 (2007).

⁵Y. Lu, J. Claude, B. Neese, Q. M. Zhang, and Q. Wang, *J. Am. Chem. Soc.* **128**, 8120–8121 (2006).

⁶N. Karawasa and W. A. Goddard, III, *Macromolecules* **25**, 7268–7281 (1992); Y. Lu, J. Claude, Q. M. Zhang, and Q. Wang, *ibid.* **39**, 6962–6968 (2006).

⁷T. Umemura, D. Couderc, and K. Akiyama, *IEEE Trans. Electr. Insul.* **21**, 137–144 (1986); J. L. Nash, *Polymer Eng. Sci.* **28**, 862–870 (1988); P. Karanja and R. Nath, *IEEE Trans. Electr. Insul.* **28**, 294–298 (1993); M. Rabuffi and G. Picci, *IEEE Trans. Plasma Sci.* **30**, 1939–1942 (2002); J. Ho, R. Ramprasad, and S. Boggs, *IEEE Trans. Dielectr. Electr. Insul.* **14**, 1295–1301 (2007).

⁸Y. D. Kondrashev and T. Gosudarst, *Inst. Priklad. Khim.* **46**, 166 (1962).

⁹Y. L. Gal'perin, Y. V. Strogalin, and M. P. Mlenik, *Vysokomol. Soed.* **7**, 933 (1965).

¹⁰J. B. Lando, H. G. Olf, and A. Peterlin, *J. Polym. Sci., Part A* **4**, 941–951 (1966).

¹¹R. Hasegawa, Y. Takahashi, O. Chatani, and H. Tadokoro, *Polym. J.* **3**, 591–600 (1972).

¹²R. Gregorio, *J. Appl. Polym. Sci.* **100**, 3272 (2006).

¹³H. Xu, Z. Cheng, D. Olsen, T. Mai, Q. M. Zhang, and G. Kavarnos, *Appl. Phys. Lett.* **78**, 2360 (2001).

¹⁴Q. M. Zhang, V. Bharti, and X. Zhao, *Science* **280**, 2101 (1998); D. Shah, P. Maiti, E. Gunn, D. F. Schmidt, D. D. Jiang, C. A. Batt, and E. P. Giannelis, *Adv. Mater.* **16**, 1173 (2004).

¹⁵D. Shah, P. Maiti, E. Gunn, D. F. Schmidt, D. D. Jiang, C. A. Batt, and E. P. Giannelis, *Adv. Mater.* **16**, 1173 (2004).

¹⁶F. Guan, J. Pan, J. Wang, Q. Wang, and L. Zhu, *Macromolecules* **43**, 384 (2010).

¹⁷L. Priya and J. P. Jog, *J. Polym. Sci. Polym. Phys.* **40**, 1682 (2002); **41**, 31 (2003); *J. Appl. Polym. Sci.* **89**, 2036 (2003).

¹⁸E. Yamada, A. Nishioka, H. Suzuki, T. Koda, and S. Ikeda, *Jpn. J. Appl. Phys.* **46**, 7371 (2007).

¹⁹D. M. Lincoln, R. A. Vaia, and R. Krishnamoorti, *Macromolecules* **37**, 4554 (2004); D. M. Lincoln, R. A. Vaia, Z. G. Wang, B. S. Hsiao, and R. Krishnamoorti, *Polymer* **42**, 9975 (2001).

²⁰K. E. Strawhecker, and E. Manias, *Chem. Mater.* **12**, 2943–2949 (2000); K. E. Strawhecker, and E. Manias, *Macromolecules* **34**, 8475–8482 (2001).

- ²¹D. Shah, P. Maiti, D. D. Jiang, C. A. Batt, and E. P. Giannelis, *Adv. Mater.* **17**, 525 (2005).
- ²²E. Manias, *Nat. Mater.* **6**, 9–11 (2007).
- ²³J. Zhang, E. Manias, and C. A. Wilkie, *J. Nanosci. Nanotechnol.* **8**, 1597–1615 (2008).
- ²⁴B. Neese, Y. Wang, B. Chu, K. Ren, S. Liu, Q. M. Zhang, C. Huang, and J. West, *Appl. Phys. Lett.* **90**, 242917 (2007).
- ²⁵J. Claude, Y. Lu, and Q. Wang, *Appl. Phys. Lett.* **91**, 212904 (2007).
- ²⁶X. Lu, A. Schirokauer, and J. Scheinbeim, *IEEE Trans. Ultrason. Ferro. Freq. Cont.* **47**, 1291–1295 (2000).
- ²⁷G. T. Davis, J. E. McKinnley, M. G. Broadhurst, and S. C. Roth, *J. Appl. Phys.* **49**, 4998 (1978).
- ²⁸A. C. Jayasuriya, A. Schirokauer, and J. I. Scheinbeim, *J. Polym. Sci., Part B: Polym. Phys.* **39**, 2793 (2001).
- ²⁹H. Sobhani, M. Razavi-Nouri, and A. A. Yousefi, *J. Appl. Polym. Sci.* **104**, 89–94 (2007).
- ³⁰Y. Huan, Y. Liu, Y. Yang, and Y. Wu, *J. Appl. Polym. Sci.* **104**, 858–862 (2007).
- ³¹A. Salimi and A. A. Yousefi, *Polym. Test.* **22**, 699 (2003).
- ³²M. Latour, K. Anis and R. M. Faria, *J. Phys. D* **22**, 806–808 (1989).
- ³³H. Sassabe, S. Saito, M. Ashahina and H. Kakutani, *J. Polym. Sci. Part A* **7**, 1405–1414 (1969).
- ³⁴V. J. McBrierty, D. C. Douglass and T. A. Weber, *J. Polym. Sci. Polym. Phys. Ed.* **14**, 1271–1286 (1976).
- ³⁵V. Tomer, G. Polizos, C. A. Randall, and E. Manias, *J. Appl. Phys.* **109**, 074113 (2011).
- ³⁶V. Tomer and C. A. Randall, *J. Appl. Phys.* **104**, 074106 (2008).
- ³⁷T. Furukawa, M. Date, and E. Fukada, *J. Appl. Phys.* **51**, 1135 (1980).
- ³⁸H. von Seggern, M. Hoschkara, M. T. de Figueiredo, J. A. Giacometti, and G. F. L. Ferreira, in *Proceedings of the 10th International Symposium On Electrets (ISE10), 22–24 September 1999* (IEEE, Athens, Greece, 1999), pp. 639–642.
- ³⁹The calculated value of permittivity for 10 wt. % composite at high fields (≈ 11) shows a similar value as experimentally measured at low fields.
- ⁴⁰W. Eisenmenger and M. Haardt, *Solid State Commun.* **41**, 917 (1982); M. Womes, E. Bihler, and W. Eisenmenger, *IEEE Trans. Electr. Insul.* **24**, 461–468 (1989); G. Eberle, E. Bihler, and W. Eisenmenger, in *Annual Report Conference on Electrical Insulation and Dielectric Phenomena* (IEEE, Pocono Manor, PA, 1990), pp. 41–46; E. Bihler, G. Neumann, G. Eberle, and W. Eisenmenger, *ibid.*, pp. 140–145; W. Eisenmenger, H. Schmidt, and B. Dehlen, *Braz. J. Phys.* **29**, 295 (1999); H. von Seggern and S. N. Fedosov, *Appl. Phys. Lett.* **81**, 2830 (2002); H. von Seggern and S. N. Fedosov, *ibid.* **91**, 062914 (2007); F. Guan, Z. Yuan, E. W. Shu, and L. Zhu, *ibid.* **94**, 052907 (2009).
- ⁴¹M. Ieda, *IEEE Trans. Dielectr. Electr. Insul.* **15**, 206 (1980).
- ⁴²V. Tomer, C. Randall, G. Polizos, J. Kostelnick, and E. Manias, *J. Appl. Phys.* **103**, 034115 (2008).
- ⁴³M. Lines and A. Glass, *Principles and Applications of Ferroelectrics and Related Materials* (Clarendon, Oxford, 1977).
- ⁴⁴Y. Takahashi, *J. Macromol. Sci. Phys., B* **37**, 421 (1998).
- ⁴⁵P. Khanchaitit and Q. Wang, *High Field Performance of Free-Radical Cross-Linked P(VDF-CTFE) Copolymers* (in preparation).